This article has been accepted for publication in a future issue of this journal, but has not been fully edited. Content may change prior to final publication. Citation information: DOI 10.1109/JLT.2015.2406392, Journal of Lightwave Technology

Extending the dynamic range of sweep-free Brillouin optical time-domain analyzer

Asher Voskoboinik, Alan E. Willner, and Moshe Tur

***Abstract*—Sweep-free Brillouin optical time-domain analysis (SF-BOTDA) replaces the sequential frequency scanning of classical BOTDA by parallel interrogation of the fiber-under-test using the simultaneous interaction of multiple pump tones with counter-propagating multiple probe tones. While the basic SF-BOTDA technique boosts the measurement speed by a factor equal to the number of probe tones used, its dynamic range is limited to approximately the pump tone spacing, which is of the order of 100MHz. This paper provides in-depth analysis of our method to significantly extend the dynamic range to the GHz regime. Based on sequential interrogation with up to three sets of multiple tones, each having a different frequency spacing, this method provides a major speed advantage over the classical BOTDA in spite of the use of three sets of tones. With this development, which does not require any additional hardware, SF-BOTDA offers distributed sensing of optical fibers over practical dynamic ranges of strain/temperature variations, with the potential to become one of the fastest sensing techniques.**

***Index Terms*— Stimulated Brillouin scattering (SBS), Brillouin sensors, optical fiber sensors, Brillouin gain spectrum (BGS).**

I. Introduction

STIMULATED Brillouin based sensors are of great interest in various security, environmental and other sensing applications [1]. Sensors based on this technology use the Brillouin nonlinear process [2] in which acoustic waves in the fiber mediate power transfer between counter propagating 'pump' and 'probe' waves. For a given pump, the spectral characteristics of the Brillouin-amplified light are uniquely tied to the local strain- and temperature-dependent acoustic velocity in the fiber. Using pulses for the pump and radar methodology, the strain and temperature distribution along optical fibers can be extracted [3].

One of the most prevalent techniques is the Brillouin Optical Time Domain Analysis (BOTDA) [4], which requires frequency sweeping of one of the counter-propagating waves in order to find the frequency difference between the pump and probe waves for which the Brillouin-mediated power transfer is maximized. This frequency is called the Brillouin Frequency Shift (BFS). The need to make consecutive multiple frequency steps in order to map the Brillouin gain spectra (BGS) and locate its maximum may potentially limit the ability to resolve fast, dynamic changes in the BFS distribution along the optical fiber.

Several dynamic Brillouin sensing concepts have been already proposed and demonstrated [5-7], including: (*i*) Slope-assisted techniques which use a single frequency to monitor how the magnitude [5-6] or phase [7] of the probe wave change as the BGS shifts with strain/temperature. While the technique is very fast, it has an inherent limited dynamic range, of the order of the width of the BGS; (*ii*) In the fast-BODTA [8] technique the optical frequency of the probe is scanned against that of the pump at high speed, limited only by the fiber length. By proper choice of the number of scanned frequencies and their spacing, an arbitrary dynamic range can be covered at a predetermined accuracy, at the expense of the time required to scan over all chosen frequencies; (*iii*) Frequency scanning was replaced in [9] by a single pulsed probe acting (in a Brillouin loss configuration) against a comb of multiple pump tones, interacting with a *single* BGS. Clearly, for good frequency resolution the pump tones spacing should be a small fraction of the width of the BGS (a few tens of MHz). However, a small frequency spacing is not is compatible with frequency-hungry short probing pulses, resulting in a demonstrated spatial resolution of 12m. Recently [10-13], we described a novel concept, called SF-BOTDA (for Sweep-Free BOTDA), which retains all the advantages of the classical BOTDA technique together with the potential to be much faster. In [10] we demonstrated the basic concept, to be described below, Sec. II, where CW multiple pump and multiple probe tones pair-wise interact via the Brillouin effect in the fiber to simultaneously probe different parts of *multiple* replicas of the fiber BGS. Once the tones are detected, the Brillouin amplification experienced by each of them can be determined, resulting in an accurate reconstruction of the BGS, and, consequently, in the determination of the BFS. Then in [11] we have shown, how the technique can be applied to distributed sensing faster than classical BOTDA by a factor, which could be as high as the number of simultaneous tones used. In [11] we also introduced the idea of 'sequential pulse launching', where the multiple pump pulsed tones are sequentially launched into the fiber, thereby avoiding nonlinear interactions among them, as well as overloading of the optical amplifiers. Fast measurements were demonstrated in [12]. However, one issue remained unsolved: Strain or temperature changes, which move the BFS by an amount larger than the frequency spacing between adjacent pump tones (or more) will introduce ambiguity, thereby, severely limiting the strain (temperature) dynamic range.

This paper presents a method to significantly extend the effective dynamic range of the SF-BOTDA technique to

Manuscript received July 19, 2014. Corresponding author: A. Voskoboinik (e-mail: voskoboi@usc.edu). This work was supported by Defense Security Cooperation Agency (DSCA) under contract DSCA-4440365063. The work of Moshe Tur was supported in part by THE ISRAEL SCIENCE FOUNDATION (grant No. 1380/12)

A. Voskoboinik and A. E. Willner are with Department of Electrical Engineering–Systems, University of Southern California, 3740 McClintock Avenue EEB 500, Los Angeles, California 90089, USA.

M. Tur is with School of electrical engineering, Tel Aviv University, Tel-Aviv, ISRAEL 69978.

Digital Object Identifier inserted by IEEE

This article has been accepted for publication in a future issue of this journal, but has not been fully edited. Content may change prior to final publication. Citation information: DOI 10.1109/JLT.2015.2406392, Journal of Lightwave Technology

(potentially) hundreds of degree Celsius and many thousands of mictrostrains (με), without sacrificing their obtainable resolution. Following the basic experimental demonstration of the technique in [13], its detailed theory is presented here. Section II provides a mathematical description of the basic SF-BOTDA technique and its dynamic range limitations. The proposed procedure to extend this dynamic range is described and quantitatively analyzed in Sec. III, with proofs given in the Appendix. Illustrative experimental demonstrations of the technique appear in Sec. IV, followed by a critical discussion, Sec. V, and summary, Sec. VI.

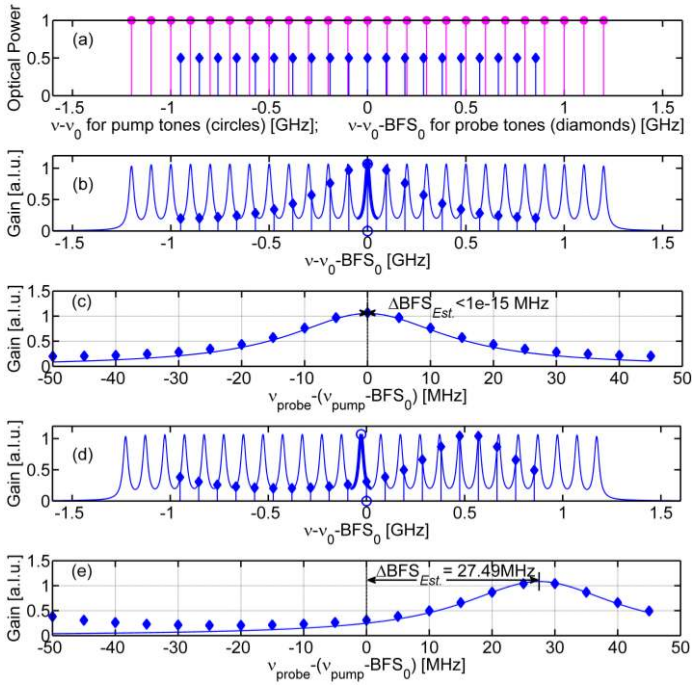

Fig. 1. Sweep-free Brillouin probing using the simultaneous launching of multiple pump and probe tones. (a) N_{pump} (=25) pump tones (Eq. (1a), magenta stems topped by circles, spaced by 100MHz) are launched into the fiber against N_{probe} (=20) probe tones (Eq. (1(b), blue stems topped by diamonds), spaced by 95MHz (*i.e.*, 5MHz smaller than that of the pump tones) and overall downshifted in frequency from the pump tones by a fixed frequency difference, BFS_0, chosen to be close to the average *BFS* of the fiber under study (note the different horizontal scales for the two stem plots); (b) The resulting cumulative Brillouin-induced gain spectrum arbitrary units ([A.U.]), generated by the pump tones together with its sampling by the probe tones. Here the actual *BFS* is assumed to be equal to BFS_0 and we note that each probe tone samples the BGS generated by the pump associated with that probe tone: *e.g.*, the middle (11th) probe tone, circled at its bottom, samples the BGS originated from the middle (13th) pump tone, bolded and circled at top; (c) Plotting the sampled gains (Diamonds) against $\{h(i)\}$ of Eq. (3) results in an approximate reconstruction of the common gain $BGS_n(\cdot)$. More importantly, fitting the upper part of the data to a parabola (not shown) produces an excellent estimation of the *zero* shift from BFS_0. A Lorentzian, precisely centered at the true $\Delta BFS=BFS-BFS_0$ and having the same height and center as the fitted parabola, is also shown in (c). The reconstructed spectrum is a bit wider than the true Lorentzian, due to the influence of neighboring peaks in (b), but shares the same peak location. (d) and (e) are the same as (b) and (c) but with BFS_0+27.5MHz. Again, the estimation of the 27.5MHz shift from BFS_0 is quite good: 27.49MHz.

II. Description Of The Original Method And Its Dynamic Range Limitation

The concept of the SF-BOTDA sensor, as described in [10-13], is illustrated in Fig. 1. Instead of scanning the frequency difference between a single pump tone and a counter-propagating single probe tone, *multiple* pump and probe tones, Fig. 1(a), are generated and counter-propagate within the optical fiber. The frequencies of the pump tones are given by:

$$\nu_{pump}(i) = \nu_0 + f_{pump}(i), \quad i = 1,\ldots,N_{pump} \tag{1}$$

Here, ν_0 is an optical frequency around which the pump frequencies reside, most commonly near 1550nm. $\{f_{pump}(i)\}$ are RF frequencies that define the pump frequencies $\{\nu_{pump}(i)\}$. $\{f_{pump}(i)\}$ can be both positive and negative; their spacing must significantly exceed the actual Brillouin linewidth in order to prevent crosstalk. In Fig. 1, $\{f_{pump}(i) = (i-1)\cdot 100 - 1200[\text{MHz}], i = 1,..,25\}$, so that the pump tones are spaced by $\Delta\nu_{pump} = 100\text{MHz}$, significantly larger than the assumed natural linewidth of 30MHz (for standard SMF fibers at around 1550nm). Note that for pump pulses shorter than ~50ns, $\Delta\nu_{pump}$ must be increased to accommodate the wider Brillouin linewidth, which approaches an inverse dependence on the pump pulse width, *T*, for *T*<20ns. These pump tones produce multiple and practically identical, [10], Brillouin gain spectra. Under common low-gain conditions, the otherwise exponential Brillouin gain, [2], can be linearized, resulting in a cumulative linear gain of the form:

$$Gain(\nu, z) = 1 + \bar{g}L\sum_{i=1}^{N_{pump}} P_i \cdot BGS_n(\nu - \nu_{pump}(i) - BFS(z)) \ . \tag{2}$$

Here, P_i [W/m^2] is the optical power density of *i-th* pump; $BGS_n(\nu)$ is a normalized Brillouin gain spectrum of Lorentzian shape for long pump pulses, and of more rounded, non-Lorentzian shape for pump pulses shorter than ~50ns; the pump-pulse-width dependent $\bar{g}$ is related to the line-center Brillouin gain factor [2], and $L=V_gT/2$ (V_g is the group velocity in the fiber). Both $\bar{g}$ and $BGS_n(\nu)$ may be a function of the distance coordinate, *z*, along the fiber. The local environmentally-sensitive down-shift in frequency, *BFS*(*z*), which is the quantity of interest [11], is assumed common to all pump tones, Fig. 1(b).

The chosen probe tones,

$$\nu_{probe}(j) = \nu_0 + f_{pump}(j+k) - BFS_0 + h(j), \quad j = 1,\ldots,N_{probe};\ N_{probe} \le N_{pump} \tag{3}$$

are a down-shifted version of the pump tones with the following distinct properties: (*i*) The downshifting amount, BFS_0, is predetermined, chosen to be close to the expected average BFS of the fiber under study; (*ii*) Since for reasons to be explained in Sec. IV the number of probe tones may be smaller than the number of pump tones (20 *vs.* 25 in all relevant figures), the parameter *k* associates the *j-th* probe tone with the (*j*+*k*)*-th* pump tone (*k*=2 in Fig. 1); and (*iii*) The spacing of the probe tones is slightly larger (or smaller) than that of the pump tones so that each probe tone samples a different region of the BGS induced by the corresponding

This article has been accepted for publication in a future issue of this journal, but has not been fully edited. Content may change prior to final publication. Citation information: DOI 10.1109/JLT.2015.2406392, Journal of Lightwave Technology

pump tone. The difference between the spacings of the tone families (5MHz in Fig. 1) eventually determines the measurement resolution, much like the frequency scanning resolution in a classical BOTDA implementation [14]. In Fig. 1, $\{h(j) = 50\text{MHz} - (j-1)\cdot 5\text{MHz},\ j = 1...20\}$, counting j from the left, and the probe tone spacing is 95MHz. In Fig. 1(b)-(c) the 'measured' *BFS* is assumed to be equal to BFS_0 (*i.e.*, zero shift) and all pump tones are of equal power. Since N_{pump}=25 while N_{probe}=20, the *j-th* tone of the probe is amplified by the (*j*+2)-*th* tone of the pump through Stimulated Brillouin Scattering (SBS). Probe tones, which are closer (in frequency) to the BGS centers, experience higher Brillouin gains. The 'measured' gains of the N_{probe} probes are then plotted, panel (c) in Fig. 1(c), against $h(\cdot)$ of (3) to obtain a line shape whose peak, denoted by ν_{shift} and calculated [14] from fitting the 30% top part of the sampled gains to a parabola (not shown), provides a measured estimate (~0MHz) of the assumed Brillouin shift of $\Delta BFS \equiv BFS - BFS_0$=0MHz. Panels (d) and (e) in Fig. 1 are the same as (b) and (c) but with a non-zero Brillouin shift, namely: $BFS = BFS_0$+27.5MHz. The observed accuracy, 27.49MHz (estimated) *vs.* 27.5MHz (assumed), is quite good (A Brillouin shift of 10kHz is related to temperature and strain variations of 0.01^0C and 0.2με, respectively). However, the ubiquitous presence of noise, ignored in the example, will undoubtedly require better frequency resolution for the same accuracy.

In this way and without the need for frequency sweeping, the SF-BOTDA technique estimates the *BFS* shift from BFS_0 in a single measurement (up to averaging), and therefore, has the potential to increase the measurement speed by a factor of N_{probe} with respect to classical BOTDA [10-13].

Note that in Fig. 1(e) (ΔBFS=27.5MHz) the first probe tone on the left (*j*=1) is no longer amplified by its corresponding pump tone (*i*=*j*+2=3), as in Fig. 1(b), but rather by the 4th pump tone. This behavior, which is also shared by probe tones *j*=2-6, worsens as ΔBFS approaches 50MHz (half the pump spacing) and is the source of ambiguity to be discussed below.

The spacing of the probe tones could be also chosen to be larger than that of the pump tones. In this case, the distances, $\{h(\cdot)\}$, (3), of the probe signals from the centers of the BGSs induced by their corresponding pump tones progressively *increase*. Note that an increasing (decreasing) *BFS* moves the cumulative Brillouin spectra to the left (right), see Fig. 1. Consequently, for increasing $h(i)$, the reconstructed Brillouin gain, Fig. 2(e), will be shifted to a negative value -27.49MHz, which is the opposite of the true shift. Since this behavior is systematic, then when working with probe tone spacing larger than that of the pump tones, the *negative* of the *observed* shift should be taken as the true value.

The above implementation of the multiple pump/probe concept works well when most probe tones are amplified by their corresponding pump tone, as in Fig. 1, where the local *BFS* deviates from BFS_0 by less than half the pump frequency spacing. Otherwise, and in view of the periodicity of the pump spectrum, the reconstruction algorithm described above generates values for the shift of the reduced spectrum, ν_{shift}, which relate to the true *BFS* shift through a *periodic* expression (the 'round(·)' function rounds its argument towards the nearest integer):

$$\nu_{shift} = \Delta BFS - n_0 \Delta\nu_{pump};\quad n_0 = \text{round}\,(\Delta BFS / \Delta\nu_{pump}) \qquad (4)$$

Indeed, for deviations of the *BFS* larger than half the pump spacing, probe tones are amplified by the Brillouin gain induced by higher-index or lower-index (in frequency) pump tones, Fig. 2. Thus, *different BFS* values separated by an integer multiple of the pump spacing produce the same reduced BGS as shown in Fig. 2. Consequently, the above-described implementation of the technique provides reliable measurements only if it is known in advance that the expected dynamic range of the strain/temperature variation in a given scenario is strictly limited to the rather small span of $\{|\Delta BFS = BFS - BFS_0| < \Delta\nu_{pump}/2\}$. Another consequence of large deviations of the *BFS* from BFS_0 is the loss of Brillouin gain at edge-residing probe tones, causing the estimation of the true *BFS* (modulo the pump tone spacing) to be a bit worse in Fig. 2(c), as compared with Fig. 1(c) (27.45 instead of 27.42MHz). While the estimation accuracy critically depends on the particular algorithm in use, this issue may be also addressed by having more pump tones than probe tones, as has been done above (N_{probe}=20<25= N_{pump}).

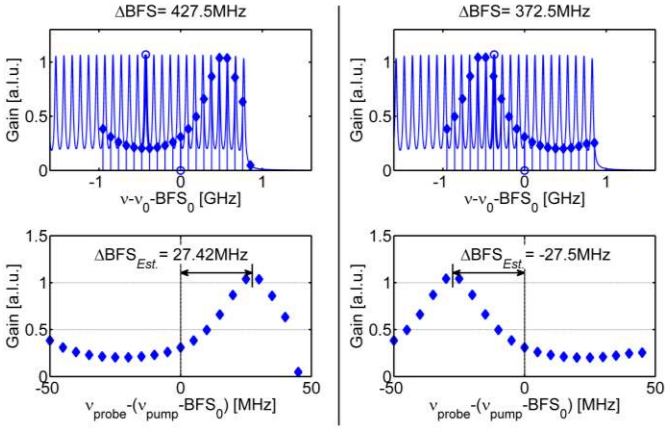

Fig. 2: Erroneous BGS reconstruction for *BFS* values which are larger than BFS_0 by more than half the pump tone spacing. Here the probe tone spacing is 95MHz as in Fig. 1. Left column: $BFS = BFS_0$+427.5MHz; Right column: $BFS = BFS_0$+372.5MHz. While the *BFS* values here are distinctly different from those of Fig. 1, they are erroneously estimated as very close to their values in Fig. 1, namely: 27.42MHz and -27.5MHz instead of 427.5 and 372.5MHz. The source of this ambiguity is the fact that the probe tones sample Brillouin gains other than those associated with them. Thus, for ΔBFS=427.5MHz (Left column) the 11th (counting from the left, circled at its bottom) probe tone does not sample the Brillouin gain induced by its corresponding pump (the 13th, bolded one, circled at top), as in Fig. 1, but rather by the (13+4)th pump tone. A similar argument holds for ΔBFS=372.5MHz.

III. Extending The Dynamic Range Of SF-BOTDA

A straightforward way to increase the dynamic range with no ambiguity is to increase the pump spacing, $\Delta\nu_{pump}$ to a value large enough to cover the required dynamic range. For example, $\Delta\nu_{pump}$ of 500MHz will cover a temperature measurement range of 500^0C or a strain dynamic range of 10,000με or a more limited combination of both. However, as detailed in [15], estimation accuracy depends on the number

This article has been accepted for publication in a future issue of this journal, but has not been fully edited. Content may change prior to final publication. Citation information: DOI 10.1109/JLT.2015.2406392, Journal of Lightwave Technology

of pump and probe tones, and for a given value of N_{pump}, the total range spanned by the pump tones, $N_{pump}\cdot\Delta\nu_{pump}$, must be smaller than the *BFS* (~11GHz). This limitation on either N_{pump} (resolution) or $\Delta\nu_{pump}$ (dynamic range) calls for more flexible ways to increase the measurement dynamic range of SF-BOTDA.

Another, although somewhat cruder, approach to deal with an arbitrary dynamic range comprises the following steps: (*i*) Determine the *BFS* using a classical BOTDA measurement (other fast methods, *e.g.* [5], also require this preliminary step to find their operating point on the BGS slope). Additional hardware is not required since our SF-BOTDA setup [10-13], is easily software-modified to act as a classical BOTDA; then (*ii*) Assign the measured value to BFS_0 ; (*iii*) perform measurements using the SF-BOTDA technique; and finally (*iv*) avoid ambiguities by continuously tracking the changes in the *BFS*, which are assumed to be much slower than the sampling rate of the SF-BOTDA technique, so that sudden jumps of the *BFS* larger than a single pump spacing, should not occur. While providing virtually unlimited dynamic range (limited only by that of the classical BOTDA instrumentation) this approach has its obvious limitations in terms of the time it consumes, as well as the difficulty to correctly determine the *BFS* under dynamic conditions [16].

Here, we propose and demonstrate an alternative novel solution, which removes the dynamic range ambiguity by employing, consecutively, pump tones of three different spacings: $\Delta\nu^{-}_{pump}<\Delta\nu^{0}_{pump}<\Delta\nu^{+}_{pump}$. Using the capabilities of our original hardware, [11-13], this reduces the sampling rate of SF-BOTDA by a factor of 3 but, somewhat surprisingly, will further increase the speed advantage of SF-BOTDA over classical BOTDA, see Sec. IV.

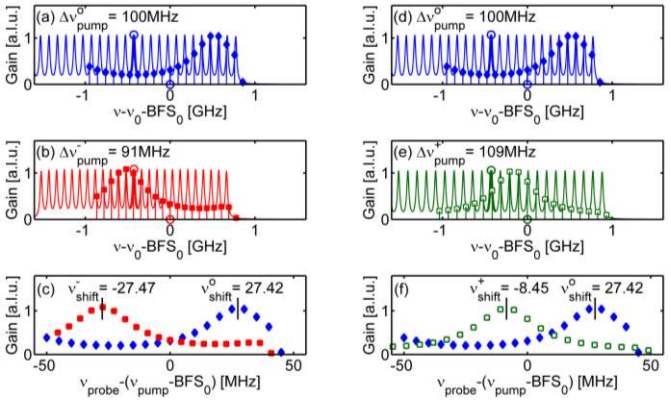

Fig. 3: BGS reconstruction of ΔBFS=427.5MHz, using 3 pump spacings for *BFS* values within the dynamic range defined by Eq. (5), which is ±450MHz (around the pre-chosen BFS_0) for the spacing choice of (a=d) $\Delta\nu^{0}_{pump}=100\text{MHz}$, (b) $\Delta\nu^{-}_{pump}=91\text{MHz}$, and (e) $\Delta\nu^{+}_{pump}=109\text{MHz}$. Once the spectral shifts of the three measurements are estimated from (c) and (f) as $\nu^{0}_{shift}=27.42$, $\nu^{-}_{shift}=-27.47$, and $\nu^{+}_{shift}=-8.45$ (all in units of MHz), n_0 and the ΔBFS can be uniquely estimated, from either the additional sampling at $\Delta\nu^{-}_{pump}$ or at $\Delta\nu^{+}_{pump}$, or from both, see text. Here only the results of the sampling at $\Delta\nu^{+}_{pump}$ are valid. Indeed, while the 11th probe samples the gain of the $(13+4)^{th}$ pump in both (a=d) and (e), it samples the gain of the $(13+5)^{th}$ pump in (b).

Each measurement, with either $\Delta\nu^{0}_{pump}$, $\Delta\nu^{-}_{pump}$ or $\Delta\nu^{+}_{pump}$ will produce an estimated shift of the reduced spectrum, panels (c) and (f) of Fig. 3, obeying equations similar to (4):

$$\begin{aligned}\Delta BFS &= n_0\Delta\nu^{0}_{pump}+\nu^{0}_{shift};\ \ n_0=\text{round}\,(\Delta BFS/\Delta\nu^{0}_{pump})\\ \Delta BFS &= n_-\Delta\nu^{-}_{pump}+\nu^{-}_{shift};\ \ n_-=\text{round}\,(\Delta BFS/\Delta\nu^{-}_{pump})\\ \Delta BFS &= n_+\Delta\nu^{+}_{pump}+\nu^{+}_{shift};\ \ n_+=\text{round}\,(\Delta BFS/\Delta\nu^{+}_{pump})\end{aligned}\qquad (5)$$

Based on these three measurements we now claim (see Appendix for proof) that the values of n_0 and consequently those of ΔBFS, Eq. (5), and ultimately those of the measured $BFS=BFS_0+\Delta BFS$, can be uniquely determined in a much wider dynamic range, *DR*, given by (the 'floor(·)' function rounds its argument towards minus infinity):

$$DR_{SF-BOTDA}=\left\{\left|BFS-BFS_0\right|<(n_{\max}+0.5)\Delta\nu^{0}_{pump}\right\};\qquad (6a)$$

$$0<n_{\max}\equiv\text{floor}\left\{0.5\min\left[\frac{\Delta\nu^{\pm}_{pump}}{\left|\Delta\nu^{0}_{pump}-\Delta\nu^{\pm}_{pump}\right|}\right]\right\}-1\qquad (6b)$$

In the example of Fig. 3, $\Delta\nu^{0}_{pump}$=100MHz, $\Delta\nu^{-}_{pump}$=91MHz, $\Delta\nu^{+}_{pump}$=109MHz so that $n_{\max}$=floor[0.5min(91/9,109/9)]-1=4. Here, the dynamic range is: $|\Delta BFS|$<450MHz, *i.e.*, 9 times wider than the previous 50MHz, and $DR_{SF-BOTDA}$=900MHz. Hence, as long as the actual strain/ temperature variations to be measured induce Brillouin frequency shifts within this range, the SF-BODTA technique provides both fast and unique results.

As shown in the Appendix, n_0 is determined from the measured $\nu^{0}_{shift}, \nu^{-}_{shift}, \nu^{+}_{shift}$ using either

$$n_0=\text{round}\left[\frac{\nu^{-}_{shift}-\nu^{0}_{shift}}{\Delta\nu^{0}_{pump}-\Delta\nu^{-}_{pump}}\right]\qquad (7.1)$$

or

$$n_0=\text{round}\left[\frac{\nu^{+}_{shift}-\nu^{0}_{shift}}{\Delta\nu^{0}_{pump}-\Delta\nu^{+}_{pump}}\right],\qquad (7.2)$$

which ever produces a value of n_0 *smaller* or *equal* in absolute value to $n_{\max}$ of (6b). Obtained values for n_0, which are *larger* than $n_{\max}$ are *discarded*. It is guaranteed, however, that as long as

$$n_{\max}<\text{floor}\left[0.5(\Delta\nu^{-}_{pump}+\Delta\nu^{+}_{pump})/(\Delta\nu^{+}_{pump}-\Delta\nu^{-}_{pump})\right]\qquad (8)$$

(=5 in our example), either (7.1) or (7.2) (or both) will provide the correct value for n_0, see Appendix. For the example of Fig. 3, the smaller, 91MHz, pump tone spacing, gives $n_0=\text{round}\,[(-27.47-27.42)/(+9)]=-6$, whose absolute value is larger than $n_{\max}$=4, and, therefore, is discarded. On the other hand, the larger pump tone separation, 109MHz, gives n_0=round[(-8.45-27.42)/(-9)]=4, resulting (see Eq. (5)) in ΔBFS_{est}=4·100+ 27.42=427.42 MHz, which is a very good estimate of the true 427.5MHz one.

This article has been accepted for publication in a future issue of this journal, but has not been fully edited. Content may change prior to final publication. Citation information: DOI 10.1109/JLT.2015.2406392, Journal of Lightwave Technology

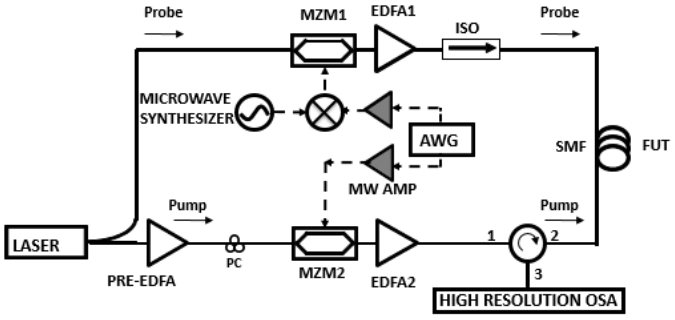

Fig. 4: Experimental block diagram: MZM: Mach-Zehnder electro-optic modulator; EDFA: Erbium-doped fiber amplifier; PC: polarization controller; ISO: optical isolator; AWG: arbitrary waveform generator; FUT: fiber-under-test.

IV. An Experimental Example

In order to illustrate the proposed concept of dynamic range extension, we used a simplified version of the experimental setup of [11-13], see Fig. 4. A highly coherent laser was split into pump and probe arms: (*i*) *Pump tones*: One channel of a wideband arbitrary waveform generator (AWG) was used to generate a comb of 10 RF frequencies, having a programmable spacing, $\Delta\nu_{pump}$. After proper RF amplification this comb drove a Mach-Zehnder electro-optic modulator (MZM2), biased near zero transmission, to produce N_{pump}=21 optical *pump* tones (the 11th tone was the laser light); (*ii*) *Probe tones:* The other channel of the AWG generated another 8-tone comb, with a programmable spacing of $\Delta\nu_{probe}$. This comb signal fed the IF input of a mixer, whose RF input was connected to a microwave synthesizer. The output of the mixer thus comprised 16 tones symmetrically arranged around the (also programmable) generator frequency. This multi-tone signal drove another modulator (MZM1), where it was up-converted to the optical domain, thereby creating two sidelobes, with N_{probe}=17 optical tones on each side of the laser light. After proper optical magnification the pump and probe signals entered the 95m single mode fiber under test (FUT) from its opposite sides. The emerging probe tones then passed a circulator on their way to a high resolution (20MHz) optical spectrum analyzer. Finally, the Brillouin gains of the amplified lower-sidelobe probe tones were estimated by measuring their optical powers with and without the pump tones. While this simplified setup, using CW rather than pulsed pump tones, cannot perform distributed sensing, it is comprehensive enough to demonstrate the proposed dynamic range extension technique.

We used the same 3 sets of pump spacing as in Figs. 1-3: $\Delta\nu_{pump}$=100, 91 and 109 MHz. The probe tones spacing, though, had to be changed to accommodate their smaller number. For the 17 probe tones to fully cover the pump tone spacing the following corresponding values were used: 93.75, 85.3125 and 102.1875 MHz, resulting in an interrogation resolution of ($\Delta\nu_{pump}$ /16) 6.25, 5.6875 and 6.8125 MHz, respectively.

With the above choice of pump spacings the allowed dynamic range is ±450 MHz, which translates into an extremely wide dynamic range of either temperature (1 MHz/^{0}C) or strain (500 MHz/1%). Instead of subjecting the fiber to extreme environments, we have used a completely equivalent and quite a simple way to experimentally test the available dynamic range.

We first turned off the AWG and scanned the microwave synthesizer to find out that maximum Brillouin gain was achieved when the synthesizer was set to $f_{osc}=BFS_{fiber}$=10,058 MHz. Then, in order to challenge the SF-BOTDA setup with a *BFS* change of ΔBFS we simply moved the synthesizer frequency from f_{osc}=10,058 MHz to $f_{osc}-\Delta BFS$. In this way, a situation was created where the setup is set to (see Sec. II) $BFS_0 = BFS_{fiber} - \Delta BFS$ and measures a fiber whose *BFS* is ΔBFS away from the frequency to which the setup was set: $\Delta BFS = BFS_{fiber} - BFS_0$.

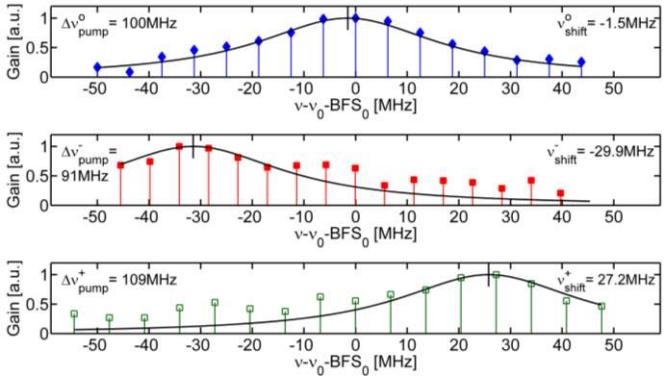

Fig. 5: Experimental demonstration of the dynamic range extension concept using three different pump tone spacings of 100, 91 and 109 MHz. 16 probe tones are used (the 17-th probe tone periodically repeats the effect of the first one). The estimated peak locations are indicated by short vertical lines and their frequency locations also appear in the figure). Based on these estimates, Lorentzian curves have been added.

Figure 5 describes the results of a measurement where the synthesizer frequency was set to 10,360MHz, being equivalent to a ΔBFS of -302 MHz. This value is well outside the native dynamic range of ~±50 MHz for the selected pump spacings. Parabolic fitting around the peaks, [14], resulted in $\nu^0_{shift} = -1.5$, $\nu^-_{shift} = -29.9$, $\nu^+_{shift} = 27.2$ MHz. Here, both Eqs. (7) give valid values for n_0=-3. ΔBFS can now be estimated in three ways:

$$\begin{aligned}\Delta BFS &= (-3)\cdot 100 + (-1.5) = -301.5 \text{ MHz}\\ \Delta BFS &= (-3)\cdot 91 + (-29.9) = -302.9 \text{ MHz},\\ \Delta BFS &= (-3)\cdot 109 + (27.2) = -299.8 \text{ MHz}\end{aligned} \qquad (9)$$

having a mean of -301.4 MHz instead of the set value of -302MHz. This obtained accuracy is well within the measurement granularity of $\Delta\nu_{pump}$/16~6 MHz.

A similar measurement was taken for the case of ΔBFS=-520MHz, which is outside the projected dynamic range of ±450 MHz. The resulting shifts were measured to be $\nu^0_{shift} = -21.3(-20)$, $\nu^-_{shift} = 25.5(26)$, $\nu^+_{shift} = 27.6(25)$ MHz (the numbers in parentheses are those predicted by Eqs. (5)). Applying Eqs. (7.1) and (7.2) we indeed get for n_0 values (5 and -5, respectively), both exceeding (in absolute values) the allowed n_{max}=4 of Eq. (6b).

While demonstrated here for the non-distributed CW version of SF-BOTDA, the proposed dynamic range extension technique is fully compatible with complete distributed-measurement-capable setup of [11-13].

This article has been accepted for publication in a future issue of this journal, but has not been fully edited. Content may change prior to final publication. Citation information: DOI 10.1109/JLT.2015.2406392, Journal of Lightwave Technology

V. DISCUSSION

A few important characteristics of the dynamic extension technique are discussed below:

(a) **How wide can the extended dynamic range $DR_{SF\text{-}BOTDA}$ go**? Clearly, the dynamic range of Eqs. (6) is inversely proportional to the difference $|\Delta\nu^{0}_{pump}-\Delta\nu^{\pm}_{pump}|$. However, the dynamic range cannot be increased at will by simply choosing $\Delta\nu^{\pm}_{pump}$ to be arbitrarily close to $\Delta\nu^{0}_{pump}$. As evident from Eqs. (6) and Fig. 3, the smaller $|\Delta\nu^{0}_{pump}-\Delta\nu^{\pm}_{pump}|$, the closer together are the measured values for $\{\nu^{0}_{shift},\nu^{\pm}_{shift}\}$ and their accurate estimation, and more importantly the accurate estimation of their difference, $\nu^{0}_{shift}-\nu^{\pm}_{shift}$, later used in Eqs. (7), becomes more difficult. Practically, a lower bound on the proximity of $\Delta\nu^{\pm}_{pump}$ to $\Delta\nu^{0}_{pump}$ will be determined by the measurement resolution (which is of the order of a fraction of the difference between the pump and probe spacings: $\Delta\nu_{spacing}\equiv|\Delta\nu^{0,\pm}_{pump}-\Delta\nu^{0,\pm}_{probe}|$), noise issues, and the sophistication of the signal processing techniques used to determine $\{\nu^{0}_{shift},\nu^{\pm}_{shift}\}$.

(b) **Speed advantage of the extended dynamic range SF-BOTDA over classical BOTDA:** In a measurement scenario involving Brillouin frequency shifts limited to $|BFS-BFS_0|<\Delta\nu_{pump}/2$ for a pre-chosen BFS_0, the original SF-BOTDA technique [10-12] offers a speed increase by a factor of N_{probe}, assuming both methods use the same number of interrogating tones with the same frequency spacing, $\Delta\nu_{spacing}$. We now show that the extended dynamic range technique of this paper offers a significantly higher gain in speed. For the same dynamic range, *DR*, and the same frequency spacing of the interrogating tones, $\Delta\nu_{spacing}$, classical BOTDA requires the sequential measurements of $DR/\Delta\nu_{spacing}$ frequencies. On the other hand, the SF-BOTDA technique will provide the same frequency coverage with the same frequency resolution in only 3 measurements! In our example of $\Delta\nu_{spacing}$=5MHz and *DR*=900MHz, the speed gain is 180/3=60 (180=900/5). Averaging will reduce the speed of both methods in the same way. This comparison assumes, though, that the more complex implementation of SF-BOTDA will provide the same signal to noise ratio as in classical BOTDA. Streamlining and optimizing the current hardware may come close to this challenging goal.

(c) **The need for extra pump tones:** It has been already noted above, Fig. 2(a-b), that every shift of the *BFS* by one pump spacing further distances one of the extreme probe tones from the BGS induced by its counter-part pump tone: While in Fig. 1 the 20th probe tone is amplified by its associated 22nd pump tone, in Fig. 2(a) the 19th probe is amplified by the 25th pump tone and the far-right 20th probe tone, which is supposed to be amplified non-existing pump tone, is not amplified at all. Unless more pump tones are added, these extreme probe tones will experience no gains, deteriorating the accuracy of the estimation of *BFS* shift. To maintain the measurement accuracy of the zero-order dynamic range ($|\Delta BFS|<\Delta\nu^{0}_{pump}/2$) over the full dynamic range of Eq. (6), N_{pump} should exceed $N_{probe}+2n_{\max}$ (In Fig. 2(a) ΔBFS=427.5MHz<450MHz, N_{pump} should have been 27. Instead, only 25 pump tones were used in order to demonstrate the issue).

(d) **The correct estimation of ν_{shift}** : Finally, the accurate estimation of the spectral shift of the reduced spectrum, ν_{shift}, is of paramount importance for the success of the SF-BOTDA method. So far, we assumed the reduced spectrum to have a well-defined peak, which is the case as long as $|\nu_{shift}|$ is not too close to $\Delta\nu^{0,\pm}_{pump}/2$, *i.e.*, not too close to the edges of the reduced spectrum, Fig. 1(c,e). In the vicinity of $\pm\Delta\nu^{0,\pm}_{pump}/2$, however, there is no distinct peak and more advanced signal processing of the data is required, probably eased by the method capability to continuously track the changes in the BFS, as well by the fact that the shape of the measured spectrum is known.

VI. SUMMARY

This paper provides an in-depth quantitative analysis of a proposed technique, which significantly extends the strain/temperature dynamic range of SF-BODTA. It shows that by performing at most three sequential measurements, each with a different frequency spacing of the multiple pumps and their corresponding multiple tones, the Brillouin Frequency Shift can be uniquely determined within an extended dynamic range, whose value depends on the chosen three frequency spacings, Eq. (5). The closer these spacings, the wider is the dynamic range. The available signal-to-noise ratio, the number of averages used and other system parameters will set a lower practical bound on their closeness. Neither the *BFS* estimation accuracy nor the spatial resolution are compromised by this dynamic-range extension technique, which neither requires any additional hardware. While the sensing speed is reduced by (at most) a factor of three (relative to the original SF-BOTDA implementation), its speed advantage over classical BOTDA is even more pronounced in many wide dynamic range applications. To alleviate the three-fold speed reduction, an alternative way to extend the dynamic range of SF-BOTDA by removing the ambiguity of what pump amplifies a given probe, is currently under study using individual coding of the pump tones.

With this development, SF-BOTDA offers distributed sensing of optical fibers over practical dynamic ranges of strain/temperature variations, with the potential to become one of the fastest sensing techniques. It is currently hardware-intensive but its speed advantages may merit the effort.

This article has been accepted for publication in a future issue of this journal, but has not been fully edited. Content may change prior to final publication. Citation information: DOI 10.1109/JLT.2015.2406392, Journal of Lightwave Technology

VII. APPENDIX

Starting from Eq. (5),

$$\begin{aligned}\Delta BFS &= n_0\Delta\nu^0_{pump}+\nu^0_{shift};\ n_0=\text{round}\,(\Delta BFS/\Delta\nu^0_{pump})\\ \Delta BFS &= n_-\Delta\nu^-_{pump}+\nu^-_{shift};\ n_-=\text{round}\,(\Delta BFS/\Delta\nu^-_{pump})\\ \Delta BFS &= n_+\Delta\nu^+_{pump}+\nu^+_{shift};\ n_+=\text{round}\,(\Delta BFS/\Delta\nu^+_{pump})\end{aligned} \quad \text{(A1)}$$

we note that since $\Delta\nu^-_{pump}<\Delta\nu^0_{pump}<\Delta\nu^+_{pump}$, the three indices $\{n_0, n_-, n_+\}$ may not be equal. If however, $n_-=n_0$ or $n_+=n_0$, then (A1) leads to:

$$n_0\Delta\nu^0_{pump}+\nu^0_{shift}=n_0\Delta\nu^\pm_{pump}+\nu^\pm_{shift}\rightarrow n_0=\frac{\nu^\pm_{shift}-\nu^0_{shift}}{\Delta\nu^0_{pump}-\Delta\nu^\pm_{pump}}\ . \quad \text{(A2)}$$

While n_0 is an integer, measurement errors and noise will cause the ratio in (A2) to slightly deviate from a whole number. Adding the round(·) function (rounding to the nearest integer) produces Eqs. (7).

But it may well be the case that $n_\pm$ measured through (A1) is different than n_0, namely: $n_\pm=n_0+m_\pm$, with $m_\pm\neq0$. We now investigate this situation and show that for the dynamic range defined by Eqs. (6), only those obtained values for $n_\pm$ which are smaller or equal in absolute value to $n_{\max}$ of (6.1) can be used to predict n_0. Furthermore, once Eq. (8) is satisfied, see below for a proof, it is guaranteed that either n_+ and/or n_- will produce the correct $n0$.

When $n_\pm=n_0+m_\pm$, with $m_\pm\neq0$, (A1) gives:

$$\begin{aligned}&n_0\Delta\nu^0_{pump}+\nu^0_{shift}=(n_0+m_\pm)\Delta\nu^\pm_{pump}+\nu^\pm_{shift}\longrightarrow\\ &\frac{\nu^\pm_{shift}-\nu^0_{shift}}{\Delta\nu^0_{pump}-\Delta\nu^\pm_{pump}}=n_0-m_\pm K_\pm;\ K_\pm\equiv\frac{\Delta\nu^\pm_{pump}}{\Delta\nu^0_{pump}-\Delta\nu^\pm_{pump}}\end{aligned} \quad \text{(A3)}$$

Our proposed procedure aims at estimating n_0 from either

$$n_0^{est-}\equiv\text{round}\left[\frac{\nu^-_{shift}-\nu^0_{shift}}{\Delta\nu^0_{pump}-\Delta\nu^-_{pump}}\right]=\text{round}\,[n_0-m_-K_-] \quad \text{(A4.1)}$$

or

$$n_0^{est+}\equiv\text{round}\left[\frac{\nu^+_{shift}-\nu^0_{shift}}{\Delta\nu^0_{pump}-\Delta\nu^+_{pump}}\right]=\text{round}\,[n_0-m_+K_+]\ . \quad \text{(A4.2)}$$

Clearly, if $m_\pm\neq0$ then $n_0^{est\pm}\neq n_0$ and the use of (A4.1-4.2) to predict the correct value of n_0 simply fails. We now prove that whenever the measurement scenario is such that the *BFS* variations do not exceed the dynamic range of (6), there is a way to detect those cases for which $m_\pm\neq0$, and to successfully avoid them.

Claims:

A) If $|n_0|\le n_{\max}\equiv\text{floor}\,\{0.5\min[|K_\pm|]\}-1$, as in (6); and if $m_\pm\neq0$, then $|n_0^{est\pm}|>n_{\max}$ and, hence, can be discarded.

B) If also $n_{\max}\le\text{floor}[0.5(\Delta\nu^-_{pump}+\Delta\nu^+_{pump})/(\Delta\nu^+_{pump}-\Delta\nu^+_{pump})]$, Eq. (8), then it is guaranteed that either $n_0=n_-$, and/or $n_0=n_+$, so that n_0 can be always correctly estimated

Proof: From our assumption that $|n_0|\le n_{\max}\equiv\text{floor}\,\{0.5\min[|K_\pm|]\}-1$ and the definition of the 'floor' function (y=floor(y)+δ, $0\le\delta<1$) it follows that

$$-0.5\min[|K_\pm|]+\delta+1\le n_0\le0.5\min[|K_\pm|]-\delta-1\ , \quad \text{(A5)}$$

with $0\le\delta<1$. The following expressions apply to $|K_+|$ if $|K_+|\le|K_-|$ or else to $|K_-|$. Thus,

$$-0.5|K_\pm|+\delta+1\le n_0\le0.5|K_\pm|-\delta-1\ . \quad \text{(A6)}$$

We now subtract $m_\pm K_\pm$ from (A6) and use the definition of the round(·) function (y=round(y)+ε, $|\varepsilon|\le0.5$) to obtain:

$$n_0-m_\pm K_\pm\begin{cases}\le+0.5|K_\pm|-m_\pm K_\pm-\delta-1\\ \ge-0.5|K_\pm|-m_\pm K_\pm+\delta+1\end{cases}$$

or

$$\left(\text{round}\,[n_0-m_\pm K_\pm]+\varepsilon\right)\begin{cases}\le+0.5|K_\pm|-m_\pm K_\pm-\delta-1\\ \ge-0.5|K_\pm|-m_\pm K_\pm+\delta+1\end{cases}$$

And finally,

$$\text{round}\,[n_0-m_\pm K_\pm]\begin{cases}\le+0.5|K_\pm|-m_\pm K_\pm-\delta-\varepsilon-1\\ \ge-0.5|K_\pm|-m_\pm K_\pm+\delta-\varepsilon+1\end{cases} \quad \text{(A7)}$$

If $m_\pm K_\pm>0$ then ($m_\pm\neq0$ is an integer whose absolute value is assumed to larger or equal to 1):

$$\begin{aligned}n_0^{est\pm}=\text{round}\,[n_0-m_\pm K_\pm]&\le0.5|K_\pm|-m_\pm K_\pm-\delta-\varepsilon-1\\ &\le\{-0.5|K_\pm|+\delta+1\}-2\delta-\varepsilon-2\\ &=-n_{\max}-(2+2\delta+\varepsilon)\end{aligned}$$

Since $(2+2\delta+\varepsilon)>0$ we conclude that

$$n_0^{est\pm}=\text{round}\,[n_0-m_\pm K_\pm]<-n_{\max}. \quad \text{(A8)}$$

Similarly, if $m_\pm K_\pm<0$ then

$$\begin{aligned}n_0^{est\pm}=\text{round}\,[n_0-m_\pm K_\pm]&\ge-0.5|K_\pm|-m_\pm K_\pm+\delta-\varepsilon+1\\ &\ge\{+0.5|K_\pm|-\delta-1\}+2\delta-\varepsilon+2\\ &=n_{\max}+(2+2\delta-\varepsilon)\\ &>n_{\max}\end{aligned} \quad \text{(A9)}$$

which completes the proof of our claim whenever $|n_0^{est+}|\le n_{\max}$ or $|n_0^{est-}|\le n_{\max}$ they can serve as valid estimators for n_0.

In order to prove our second claim we plot in Fig. A1 the ΔBFS dependence of n_0, Eqs. (7) (blue: solid), n_0^{est-} (red: dashed) and n_0^{est+} (green: dashed-dotted), Eq. (A4), for the data of the pump tone spacings used in Fig. 3. Also shown are vertical arrows, denoting the allowed dynamic range of Eqs. (6), $|\Delta BFS|\le450$MHz, and horizontal arrows at vertical values of $\pm n_{\max}$. It is clearly seen that as long as ΔBFS is within its dynamic range, a correct estimate of n_0 can always

This article has been accepted for publication in a future issue of this journal, but has not been fully edited. Content may change prior to final publication. Citation information: DOI 10.1109/JLT.2015.2406392, Journal of Lightwave Technology

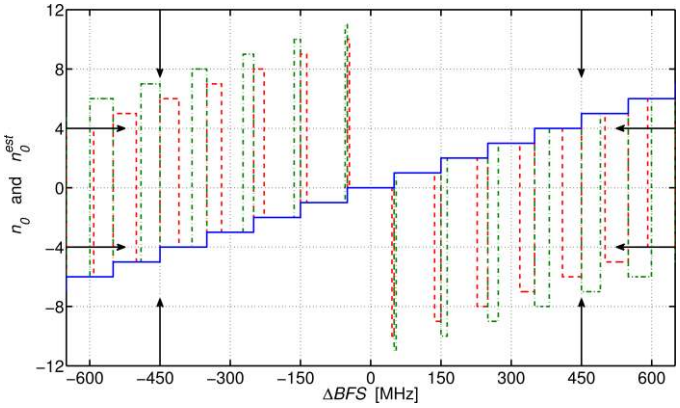

Fig. A1. The dependence of n_0 (blue: solid), n_0^{est-} (red: dashed) and n_0^{est+} (green: dashed-dotted), Eq. (A4), on ΔBFS for the data of the pump tone spacings used in Fig. 4: $\Delta\nu_{pump}^{0}=100\text{MHz}$, $\Delta\nu_{pump}^{-}=91\text{MHz}$, and $\Delta\nu_{pump}^{+}=109\text{MHz}$. The vertical arrows denote the allowed dynamic range of Eqs. (6), $|\Delta BFS|\leq 450\text{MHz}$, while horizontal arrows point at the maximum allowed values for $\pm n_{\max}$ (±4).

be obtained from either n_0^{est-} (the red curve coincides with the blue one) or from n_0^{est+} (the green curve coincides with the blue one) or from both. As ΔBFS grows from $\Delta BFS=0$, the two estimates work well (i.e., $n_0^{est-}=n_0^{est+}=n_0=0$ until ΔBFS exceeds $\Delta\nu_{pump}^{-}/2$, where n_- becomes $1(\neq n_0=0)$, driving n_0^{est-} to a value (-10) smaller than $-n_{\max}$(-4). At this point, n_0 can be estimated only from n_0^{est+}. When ΔBFS exceeds $\Delta\nu_{pump}^{0}/2$, n_0 increases to 1 (=n_-) and n_0 can be again correctly estimated from n_0^{est-} but not from n_0^{est+} (=-11<-4). $n_0^{est-}=n_0^{est+}=n_0$ resumes its validity for $\Delta BFS\geq\Delta\nu_{pump}^{+}/2$ until ΔBFS crosses $1.5\Delta\nu_{pump}^{-}=136\text{MHz}$, and so on and so forth. This guaranteed estimation process of n_0 depends on the returning of the n_0^{est+} curve to the n_0 curve *before* the n_0^{est-} curve departs from the n_0 one. Let $\Delta BFS_{+,return}$ denote the value of ΔBFS at which the n_0^{est+} returns to the n_0 curve. Similarly, $\Delta BFS_{-,Depart}$ will denote the value of ΔBFS at which the n_0^{est-} departs from the n_0 curve. Mathematically,

$$\begin{aligned}\Delta BFS_{+,return}&\equiv n_0\Delta\nu_{pump}^{+}-\Delta\nu_{pump}^{+}/2\\ \Delta BFS_{-,depart}&\equiv n_0\Delta\nu_{pump}^{-}+\Delta\nu_{pump}^{-}/2\end{aligned}\quad . \tag{A10}$$

In order for the n_0^{est+} curve to return to the n_0 one before the departure of the n_0^{est-} curve we require that

$$\Delta BFS_{+,return}\leq\Delta BFS_{-,depart}\ , \tag{A11}$$

which leads to the additional condition on $n_{\max}$, (8), namely:

$$n_{\max}\leq\text{floor}\left[0.5\frac{\Delta\nu_{pump}^{-}+\Delta\nu_{pump}^{+}}{\Delta\nu_{pump}^{+}-\Delta\nu_{pump}^{+}}\right] \tag{A12}$$

Similar considerations hold for $\Delta BFS<0$, also resulting in (A12). In our example of Fig. 3, (A12) is violated for $|\Delta BFS|>591.5\text{MHz}$, outside our allowed dynamic range. More generally, it is easy to show that a sufficient, but by no means necessary condition for (A12) to be obeyed for $n_{\max}$ of Eq. (6b), is to choose the three pump spacings such that $\Delta\nu_{pump}^{0}$ is the average of $\Delta\nu_{pump}^{-}$ and $\Delta\nu_{pump}^{+}$.

REFERENCES

[1] X. Bao and L. Chen, "Recent progress in Brillouin scattering based fiber sensors," IEEE Sen. J., **11**, 4152-4187, (2011).
[2] R.W. Boyd, *Nonlinear Optics*, (Academic Press, 2008), Chap. 9.
[3] M. Barnoski and S. Personick, "Measurements in Fiber Optics," Proc. IEEE **66**, 429-441 (1978).
[4] S. Diaz, S. Mafang, M. Lopez-Amo, and L. Thevenaz, "A high performance Optical Time-Domain Brillouin Distributed Fiber Sensor," IEEE Sen. J., **8**, 1268-1272 (2008).
[5] R. Bernini, A. Minardo and L. Zeni., "Dynamic strain measurement in optical fibers by stimulated Brillouin scattering," Optics Letters, **34**, 2613-2615 (2009).
[6] Yair Peled, Avi Motil, Lior Yaron and Moshe Tur, "Slope-assisted fast distributed sensing in optical fibers with arbitrary Brillouin profile", Optics Express, Vol. 19, pp. 19845-19854, Oct. 2011.
[7] J. Urricelqui, A. Zornoza, M. Sagues, and A. Loayssa, "Dynamic BOTDA measurements based on Brillouin phase-shift and RF demodulation," Opt. Express **20**, 26942-26949 (2012).
[8] Yair Peled, Avi Motil, and Moshe Tur, "Fast Brillouin optical time domain analysis for dynamic sensing," Optics Express, Vol. 20, pp. 8584-8591 (2012).
[9] P. Chaube, B. G. Colpitts, D. Jagannathan and A.W. Brown, "Distributed Fiber-Optic Sensor for Dynamic Strain Measurement," IEEE Sen. J., **8**, 1067-1072 (2008).
[10] A. Voskoboinik, J. Wang, B. Shamee, S. Nuccio, L. Zhang, M. Chitgarha, A. Willner and M. Tur, "SBS-based fiber optical sensing using frequency-domain simultaneous tone interrogation," J. of Lightwave Techn., **29**, 1729-1735 (2011).
[11] A. Voskoboinik, O.F. Yilmaz, A.E. Willner and M. Tur, "Sweep-free distributed Brillouin time-domain analyzer (SF-BOTDA)," Optics Express, **19**, Iss. 26, B842—B847 (2011).
[12] A. Voskoboinik, D. Rogawski, H. Huang, Y. Peled, A. E. Willner and M. Tur, "Frequency-domain analysis of dynamically applied strain using sweep-free Brillouin time-domain analyzer and sloped-assisted FBG sensing," Optics Express, **20**, Iss. 26, B581-B-586 (2012).
[13] A. Voskoboinik, A. Bozovitch, A. E. Willner and M. Tur, "Sweep-free Brillouin optical time-domain analyzer with extended dynamic range," CLEO 2012, San Jose, USA (2012).
[14] M. A. Soto and L. Thevenaz, "Modeling and evaluating the performance of Brillouin distributed optical fiber sensors," Optics Express, **21**, Iss. 25, 31347-31366 (2013).
[15] A. Voskoboinik, A. E. Willner and M. Tur, "Performance analysis of the sweep-free Brillouin optical time-domain analyzer (SF-BOTDA)," Optical Fiber Sensor conference, OFS-23, Santander, Spain (2014).
[16] A. Motil, Y. Peled, Lior Yaron and M. Tur, "BOTDA measurements in the presence of fiber vibration," 3rd Asia Pacific Optical Sensor Conference (APOS 2012), Sydney, Australia (2012).